

Electronic Supplementary Information

Structural Characterization of HPM-7, a More Ordered Than Expected Germanosilicate Zeolite

Peng Lu, Yaping Zhang, Alvaro Mayoral, Luis Gómez-Hortigüela and Miguel Cambor*

Index:

Fig. S1 Rietveld plot of as-made HPM-7 ($\lambda=0.56383$ Å). Purple points: experimental, green line: calculated, blue line: difference, yellow markers: allowed reflections. The refinement is considered unsuccessful (see disagreements marked by red arrows).

Fig. S2 Stacking faults of POS-A and POS-B along a unique direction ([1-10] or [110]) has little impact on the corresponding XRD patterns, as shown here with all patterns superimposed. The inset shows the portion of the pattern where the largest changes are observed, with the experimental pattern for comparison.

Fig. S3 Simulated XRD patterns for POS-C intergrown with itself with or without a 90° rotation. The bottom and top traces correspond to 99% pure structures with a given orientation (hence both are related by a 90° shift) and are compared to the experimental HPM-7. The intermediate traces correspond to 10% increments of a given orientation. There is hardly any change in the XRD along the series and very subtle differences with POS (arrows).

Fig. S4 Different cutting planes from 3D-EDT data. Reflection rule agrees with the P42/mnm (SG: No.136): 0kl: $k+l=2n$; 00l: $l=2n$; 0k0: $k=2n$.

Table S1 29 independent 3D-EDT data sets.

Fig. S5 Cs-corrected STEM ADF analysis of HPM-7 along the [001] zone axis. a) Low-magnification image. b) Electron diffraction pattern that clearly displays the crystal extinctions (yellow arrows). c) and d) High-resolution images obtained from the edge of the crystal.

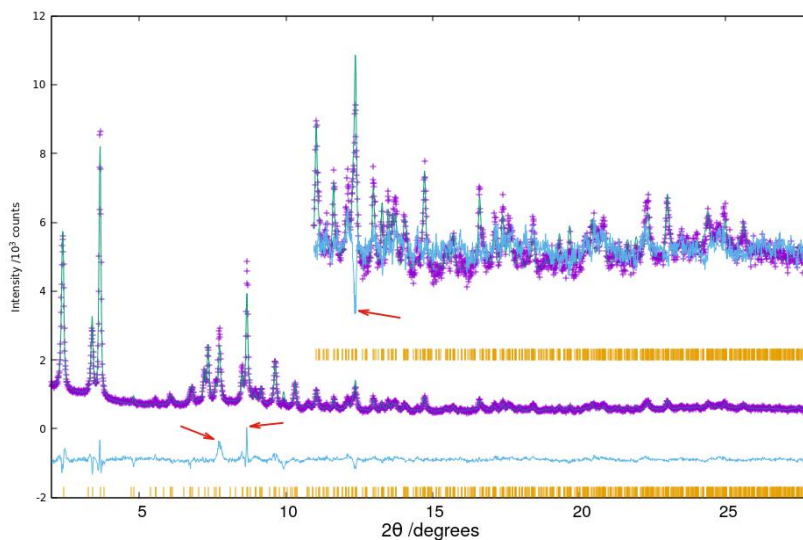


Fig. S1 Rietveld plot of as-made HPM-7 ($\lambda=0.56383 \text{ \AA}$). Purple points: experimental, green line: calculated, blue line: difference, yellow markers: allowed reflections. The refinement is considered unsuccessful (see disagreements marked by red arrows).

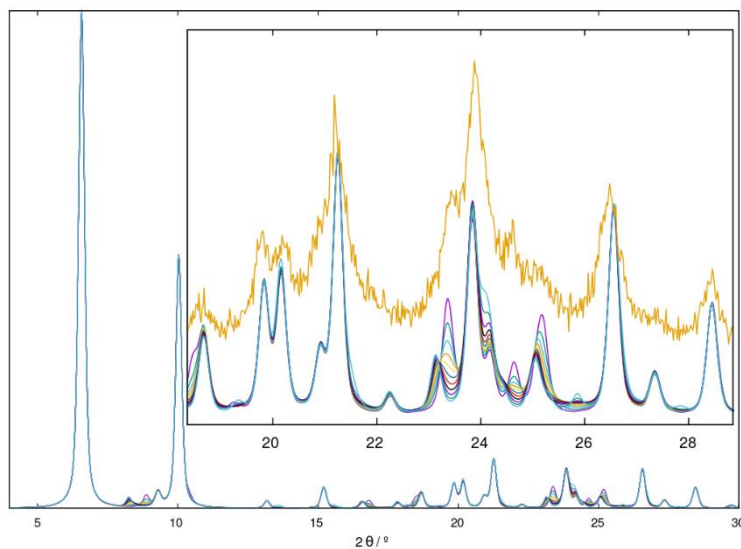


Fig. S2 Stacking faults of POS-A and POS-B along a unique direction ($[1-10]$ or $[110]$) has little impact on the corresponding XRD patterns, as shown here with all patterns superimposed. The inset shows the portion of the pattern where the largest changes are observed, with the experimental pattern for comparison.

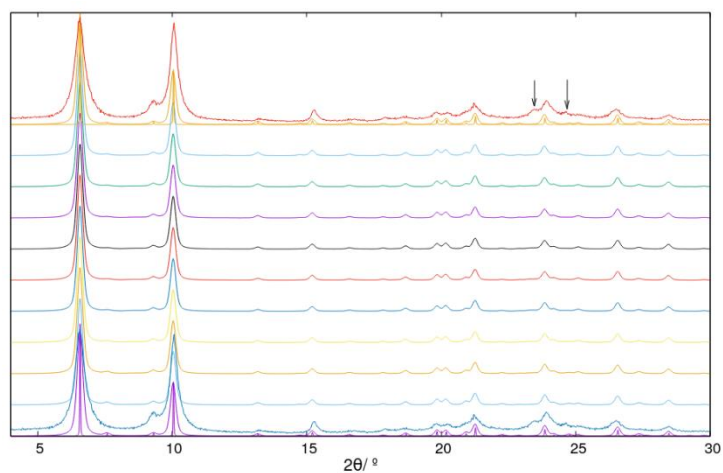


Fig. S3 Simulated XRD patterns for POS-C intergrown with itself with or without a 90° rotation. The bottom and top traces correspond to 99% pure structures with a given orientation (hence both are related by a 90° shift) and are compared to the experimental HPM-7. The intermediate traces correspond to 10% increments of a given orientation. There is hardly any change in the XRD along the series and very subtle differences with POS (arrows).

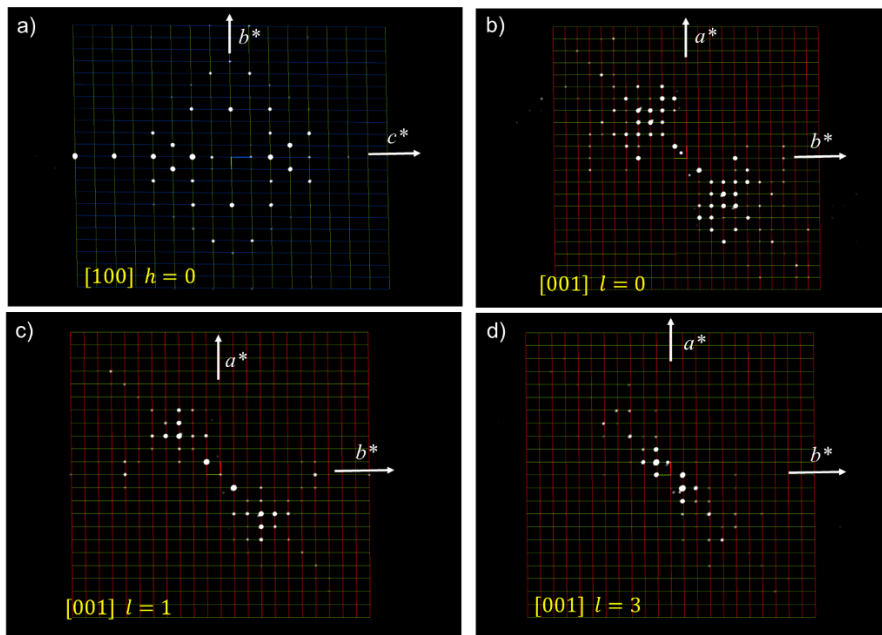


Fig. S4 Different cutting planes from 3D-EDT data. Reflection rule agrees with the P42/mmm (SG: No.136): $0kl: k+l=2n$; $00l: l=2n$; $0k0: k=2n$.

Table S1 29 independent 3D-EDT data sets

No	Resolution	$a(\text{Å})$	$b(\text{Å})$	$c(\text{Å})$	$\alpha(^{\circ})$	$\beta(^{\circ})$	$\gamma(^{\circ})$	$P4_2/mnm(136)$	Other Space Group Candidates					
1	0.9	19.332	19.354	11.823	89.475	90.043	90.988	$P4_2/mnm(136)$	$Pnmm(58)$	$Pnm2(34)$				
2	1.1	19.338	19.437	11.992	90.406	89.841	89.375	$P4_2/mnm(136)$	$P4_2,2(90)(NO)$	P- $4_2m(113)(NO)$	$P2_1,2(18)(NO)$			
3	0.9	19.271	19.323	12.013	90.757	89.519	90.025	$P4_2/mnm(136)$						
4	0.9	19.490	19.438	11.828	89.675	90.518	90.764	$P4_2/mnm(136)$						
5	0.9	19.438	19.480	11.803	90.076	90.008	90.845	$P4_2/mnm(136)$						
6	0.9	19.351	19.297	12.000	90.369	89.801	89.899	$P4_2/mnm(136)$						
7	0.9	19.475	19.417	11.859	89.544	90.533	90.241	$P4_2/mnm(136)$						
8	0.9	19.408	19.418	11.816	89.624	89.448	89.462	$P4_2/mnm(136)$						
9	0.9	19.401	19.355	11.866	90.838	89.373	89.732	$P4_2/mnm(136)$						
10	0.9	19.430	19.470	11.799	89.624	90.202	90.772	$P4_2/mnm(136)$	$Pbam(55)(NO)$	$P4_2,2(90)(NO)$	$P-4_2,m(113)$	$Pba2(32)(NO)$		
11	1.2	19.174	19.331	11.937	89.901	89.993	90.523	$P4_2/mnm(136)$	$P-4_2,m(113)$	$P4_2,2(90)(NO)$				
12	0.9	19.448	19.411	11.840	90.409	89.599	90.231	$P4_2/mnm(136)$						
13	0.9	19.479	19.395	11.807	89.223	90.241	90.619	$P4_2/mnm(136)$						
14	1.2	19.280	19.248	11.843	90.585	90.909	89.824	$P4_2/mnm(136)$						
15	0.9	19.337	19.298	11.948	89.635	89.196	89.967	$P4_2/mnm(136)$	$P4mm(99)(NO)$	P- $4_2m(111)(NO)$	$P4/mmm(123)(NO)$	$P4_2,2(90)(NO)$	P- $4_2,m(113)(NO)$	$P422(89)(NO)$
16	0.9	19.400	19.354	11.937	90.520	89.369	89.928	$P4_2/mnm(136)$						
17	0.9	19.443	19.442	11.820	90.304	90.290	89.602	$P4_2/mnm(136)$						
18	0.9	19.466	19.431	11.809	89.670	90.376	90.837	$P4_2/mnm(136)$						
19	1.0	19.350	19.288	11.993	89.906	90.329	89.688	$P4_2/mnm(136)$						
20	0.9	19.482	19.443	11.821	89.743	89.612	89.251	$P4_2/mnm(136)$						
21	0.9	19.352	19.295	11.971	89.428	90.694	89.823	$P4_2/mnm(136)$						
22	0.9	19.347	19.374	11.954	89.322	90.667	90.005	$P4_2/mnm(136)$						
23	0.9	19.356	19.331	11.984	90.574	90.618	89.874	$P4_2/mnm(136)$						
24	1.0	19.406	19.360	11.946	89.476	90.621	89.904	$P4_2/mnm(136)$	$P-4_2,m(113)$	$P4_2,2(90)(NO)$				
25	0.9	19.365	19.375	11.965	90.647	89.345	90.277	$P4_2/mnm(136)$						

26	1.0	19.412	19.473	11.883	89.299	90.612	90.253	P4 ₂ /mnm(136)						
27	0.9	19.363	19.266	11.999	90.513	89.117	90.410	P4 ₂ /mnm(136)						
28	0.9	19.325	19.433	11.888	89.999	90.734	90.043	P4 ₂ /mnm(136)						
29	0.9	19.456	19.618	11.905	90.000	88.615	90.000	P4 ₂ /mnm(136)						

“No” here means that structures failed to be reconstructed with this space group.

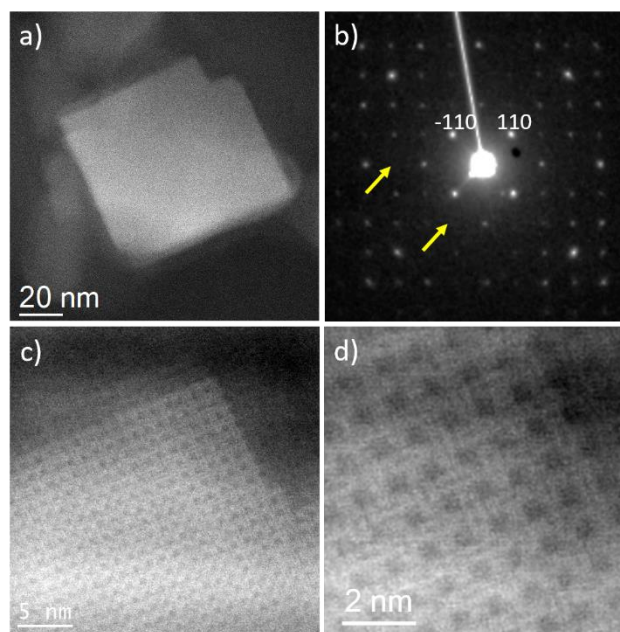


Fig. S5 Cs-corrected STEM ADF analysis of HPM-7 along the [001] zone axis. a) Low-magnification image. b) Electron diffraction pattern that clearly displays the crystal extinctions (yellow arrows). c) and d) High-resolution images obtained from the edge of the crystal.